AJ, in press
Preprint typeset using LaTeX style emulateapj v. 11/10/09

AGE AND MASS CONSTRAINTS FOR A YOUNG MASSIVE CLUSTER IN M31 BASED ON SPECTRAL-ENERGY-DISTRIBUTION FITTING

Jun Ma,[1,2] Song Wang,[1,3] Zhenyu Wu,[1] Zhou Fan,[1] Yanbin Yang,[1] Tianmeng Zhang,[1] Jianghua Wu,[1] Xu Zhou,[1] Zhaoji Jiang,[1] and Jiansheng Chen[1]

AJ, in press

ABSTRACT

VDB0-B195D is a massive, blue star cluster in M31. It was observed as part of the Beijing-Arizona-Taiwan-Connecticut (BATC) Multicolor Sky Survey using 15 intermediate-band filters covering a wavelength range of 3000–10,000 Å. Based on aperture photometry, we obtain its spectral-energy distribution (SED) as defined by the 15 BATC filters. We apply previously established relations between the BATC intermediate-band and the Johnson-Cousins $UBVRI$ broad-band systems to convert our BATC photometry to the standard system. A detailed comparison shows that our newly derived VRI magnitudes are fully consistent with previous results, while our new B magnitude agrees to within 2σ. In addition, we determine the cluster's age and mass by comparing its SED (from 3000 to 20,000Å, comprising photometric data in the 15 BATC intermediate bands, optical broad-band $BVRI$, and 2MASS near-infrared JHK_s data) with theoretical stellar population synthesis models, resulting in age and mass determinations of 60.0 ± 8.0 Myr and $(1.1 - 1.6) \times 10^5 M_\odot$, respectively. This age and mass confirms previous suggestions that VDB0-B195D is a young massive cluster in M31.

Subject headings: galaxies: individual (M31) – galaxies: star clusters – galaxies: stellar content

1. INTRODUCTION

Young massive star clusters (YMCs) are among the main objects resulting from violent star-forming episodes triggered by galaxy collisions, mergers, and close encounters (see de Grijs & Parmentier 2007, and references therein). They are also referred to as 'young populous clusters,' a term first coined by Hodge (1961), who used it to describe 23 clusters containing bright, blue stars in the Large Magellanic Cloud. In Hodge (1961), the 'young' aspect is demonstrated by the fact that all clusters have main sequences that extend to absolute magnitudes brighter than $M_V = 0$, while 'populous' describes their richness (stellar membership). However, YMCs are also observed in quiescent galaxies (Larsen & Richtler 1999) and in the disks of isolated spirals, although higher cluster-formation efficiencies are associated with environments exhibiting high star-formation rates (see Larsen 2004; Cao & Wu 2007, and references therein). It has become clear that, in many ways, YMCs resemble young versions of the old globular clusters (GCs) associated with all large galaxies (see Larsen et al. 2004, and references therein). YMCs are seemingly absent in the Milky Way; possibly the best example of a Galactic YMC is Westerlund 1, a heavily reddened cluster with an age and mass of 4–5 Myr (Crowther et al. 2006) and $M_{\rm cl} \sim 10^5\ M_\odot$ (Clark et al. 2005), respectively.

Since the pioneering work of Tinsley (1968, 1972) and Searle (1973), evolutionary population synthesis modeling has become a powerful tool to interpret integrated spectrophotometric observations of galaxies and their components, such as star clusters (e.g., Anders et al. 2004). The evolution of star clusters is usually modeled by means of the simple stellar population (SSP) approximation. An SSP is defined as a single generation of coeval stars formed from the same progenitor molecular cloud (thus implying a single metallicity), and governed by a given stellar initial mass function (IMF).

Age and metallicity are two basic star cluster parameters. The most direct method to determine a cluster's age is by employing main-sequence photometry, since the absolute magnitude of the main-sequence turnoff is predominantly affected by age (see Puzia et al. 2002, and references therein). However, until recently (cf. Perina et al. 2009), this method was only applied to the star clusters in the Milky Way and its satellites (e.g., Rich et al. 2001), although Brown et al. (2004) estimated the age of an M31 GC using extremely deep images observed with the *Hubble Space Telescope (HST)*'s Advanced Camera for Surveys. Generally, the ages of extragalactic star clusters are determined by comparing their observed spectral-energy distributions (SEDs) and/or spectroscopy with the predictions of SSP models (Williams & Hodge 2001a,b; de Grijs et al. 2003a,b,c; Bik et al. 2003; Jiang et al. 2003; Beasley et al. 2004; Puzia et al. 2005; Ma et al. 2006; Fan et al. 2006; Ma et al. 2007, 2009; Caldwell et al. 2009; Wang et al. 2010). Nevertheless, SSP models assume that cluster IMFs are fully populated, i.e., that clusters contain infinite numbers of stars with a continuous distribution of stellar masses, and that all evolutionary stages are well sampled. Real clusters, however, contain a finite number of stars. Therefore, a disagreement between the observed cluster colors and theoretical colors derived from SSP models may become apparent (see Piskunov et al. 2009; Popescu & Hanson 2010, and references therein). Other limitations inherent to SSP models arise from our poor

[1] National Astronomical Observatories, Chinese Academy of Sciences, Beijing 100012, P. R. China; majun@nao.cas.cn
[2] Key Laboratory of Optical Astronomy, National Astronomical Observatories, Chinese Academy of Sciences, Beijing 100012, P. R. China
[3] Graduate University, Chinese Academy of Sciences, Beijing 100039, P. R. China

understanding of some advanced stellar evolutionary stages, such as the supergiant and the asymptotic-giant-branch (AGB) phases (see Bruzual & Charlot 2003, and references therein).

Located at a distance of 785 ± 25 kpc, corresponding to a distance modulus of $(m - M)_0 = 24.47 \pm 0.07$ mag (McConnachie et al. 2005), M31 is the nearest and largest spiral galaxy in the Local Group of galaxies. It has been the subject of many GC studies and surveys, dating back to the early study of Hubble (1932). Based on previous publications (Hubble 1932; Seyfert & Nassau 1945; Hiltner 1958; Mayall & Eggen 1953; Kron & Mayall 1960), Vetešnik (1962) compiled the first large M31 GC catalog, containing UBV photometric data of approximately 300 GC candidates. Over the past decades, several major catalogs of M31 GCs and GC candidates have been published, including major efforts by the Bologna group (Battistini et al. 1980, 1987, 1993), Barmby et al. (2000), Galleti et al. (2004, 2005, 2006, 2007), Kim et al. (2007), Caldwell et al. (2009), and Peacock et al. (2010). Following on from the first extensive spectroscopic survey of M31 GCs by van den Bergh (1969), a significant number of authors (e.g., Huchra et al. 1982; Huchra et al. 1991; Dubath & Grillmair 1997; Federici et al. 1993; Jablonka et al. 1998; Barmby et al. 2000; Perrett et al. 2002; Galleti et al. 2006; Lee et al. 2008, and references therein) have studied their spatial, kinematic, and chemical (metallicity) properties.

M31 is known to host a large number of young star clusters (e.g., Fusi Pecci et al. 2005; Caldwell et al. 2009; Wang et al. 2010, and references therein). Fusi Pecci et al. (2005) presented a comprehensive study of 67 very blue star clusters, which they referred to as 'blue luminous compact clusters' (BLCCs). Since they are quite bright ($-6.5 \leq M_V \leq -10.0$ mag) and very young (< 2 Gyr), BLCCs may be equivalent to YMCs (see for details Perina et al. 2009, 2010). To ascertain their properties, Perina et al. (2009, 2010) performed an imaging survey of 20 BLCCs in the disk of M31 using the *HST*'s Wide Field and Planetary Camera-2 (WFPC2). They obtained the reddening values, ages, and metallicities of their sample clusters by comparing the observed color-magnitude diagrams (CMDs) and luminosity functions with theoretical models.

VDB0-B195D was first detected by van den Bergh (1969). Its color is extremely blue (e.g., $U - B = -0.48$ mag; van den Bergh 1969) and it is very bright in blue bands (e.g., $U = 14.66$ mag; van den Bergh 1969). As a consequence, van den Bergh (1969) asserted that VDB0-B195D is the brightest open cluster in M31. He determined an integrated stellar spectral type equivalent to A0, which implies that the cluster contains massive stars. In addition, VDB0-B195D is particularly extended and most previous photometric studies did not include the full extent of the object's light distribution (see for details Perina et al. 2009). We will provide an overview of previous studies that included the cluster in §2.1. It was observed as part of the galaxy calibration program of the Beijing-Arizona-Taiwan-Connecticut (BATC) Multicolor Sky Survey (e.g., Fan et al. 1996; Zheng et al. 1999) in 15 intermediate-band filters. Combined with photometry in optical broad-band $BVRI$ and near-infrared JHK_s filters from the Two Micron All Sky Survey (2MASS) taken from Perina et al. (2009), we obtained the SED of VDB0-B195D in 22 filters, covering the wavelengh range from 3000 to 20,000 Å.

In this paper, we describe the details of the observations and our approach to the data reduction in §2. In §3, we determine the age and mass of VDB0-B195D by comparing observational SEDs with population synthesis models. We discuss the implications of our results and provide a summary in §4.

2. OPTICAL AND NEAR-INFRARED OBSERVATIONS OF THE YMC VDB0-B195D

2.1. *Historical overview*

VDB0-B195D was first given the designation '0' (i.e., VDB0), the brightest open cluster in M31, in the catalog of van den Bergh (1969). Battistini et al. (1987) identified VDB0-B195D independently and called it B195D. In Battistini et al. (1987), B195D was given a low level of confidence (class D) of being a genuine cluster (classes A and B were assigned very high and high levels of confidence, respectively). It was only recently independently confirmed to be a single object. Caldwell et al. (2009) presented a new catalog containing 670 likely star clusters, stars, possible stars, and galaxies in the field of M31, all with updated high-quality coordinates accurate to $0.2''$, based on images from either the Local Group Galaxies Survey (LGGS) (Massey 2006) or the Digitized Sky Survey (DSS). They use the designation VDB0-B195D, associated with $\alpha_0 = 00^{\rm h}40^{\rm m}29^{\rm s}.43$ and $\delta_0 = +40°36'14''.8$ (J2000.0), which are the coordinates we adopt in this paper. Independently, Perina et al. (2009) studied the properties of VDB0-B195D in detail based on their *HST*/WFPC2 imaging survey of young massive GCs in M31. They initially selected VDB0-B195D as two YMCs in M31, but their WFPC2 images showed unequivocally that these two sample objects are, in fact, the same cluster. In addition, the *HST* images clearly confirmed that VDB0-B195D is a real cluster. However, it is difficult to establish whether it is more similar to ordinary open clusters, similar to those in the disk of the Milky Way, than to YMCs that may evolve to become disk GCs (see for details Perina et al. 2009). Spectral observations of VDB0-B195D were obtained by van den Bergh (1969)—yielding classification spectra and the object's radial velocity—and Perrett et al. (2002), who used them for determination of its radial velocity and metallicity.

2.2. *Archival images of the BATC Multicolor Sky Survey*

Observations of the YMC VDB0-B195D were obtained with the BATC 60/90cm Schmidt telescope located at the XingLong station of the National Astronomical Observatory of China (NAOC). This telescope is equipped with 15 intermediate-band filters covering the optical wavelength range from 3000 to 10,000 Å. The filter system was specifically designed to avoid contamination by the brightest and most variable night-sky emission lines. Descriptions of the BATC photometric system can be found in Fan et al. (1996). Before February 2006, a Ford Aerospace 2k×2k thick CCD camera was installed, with a pixel size of 15 μm and a field of view of $58' \times 58'$, yielding a resolution of $1.7''$ pixel^{-1}. Since February 2006, a

new E2V 4k×4k thinned CCD with a pixel size of 12 μm has been in operation, featuring a resolution of 1.3″ pixel^{-1}. The blue quantum efficiency of the new, thinned CCD is 92.2% at 4000 Å, which is much higher than for the old, thick device (see for details Fan et al. 2009). A field including VDB0-B195D in the a–c filters was observed with the thinned CCD, and in d–p bands with the thick CCD. Fig. 1 shows a finding chart of VDB0-B195D in the BATC g band (centered at 5795 Å), obtained with the NAOC 60/90cm Schmidt telescope. We adopt an aperture with a radius of 15″ (shown in Fig. 1) for the integrated photometry discussed in this paper.

The BATC survey team obtained 61 images of VDB0-B195D in 15 BATC filters between January 2004 and November 2006. Fan et al. (2009) performed the data reduction of these images, which formed part of their M31-7 field. Table 1 contains the observation log, including the BATC filter names, the central wavelength and bandwidth of each filter, the number of images observed through each filter, and the total observing time per filter. Multiple images through the same filter were combined to improve image quality (i.e., increase the signal-to-noise ratio and remove spurious signal).

2.3. *Intermediate-band photometry of VDB0-B195D*

We determined the intermediate-band magnitudes of VDB0-B195D on the combined images using a standard aperture photometry approach, i.e., the PHOT routine in DAOPHOT (Stetson 1987). Calibration of the magnitude zero level in the BATC photometric system is similar to that of the spectrophotometric AB magnitude system. For flux calibration, the Oke-Gunn (Oke & Gunn 1983) primary flux standard stars HD 19445, HD 84937, BD +26°2606, and BD +17°4708 were observed during photometric nights (Yan et al. 2000). VDB0-B195D is located in the M31-7 field of Fan et al. (2009). The absolute flux of the M31-7 field was calibrated based on secondary standard transformations using the M31-1 field, which was calibrated, in turn, by the four Oke-Gunn primary flux standard stars by Jiang et al. (2003). Since VDB0-B195D is an extended object, an appropriate aperture size must be adopted to determine its total luminosity. The (radial) photometric asymptotic growth curve, in all BATC bands, flattens out at a radius of $\sim$ 15″. Inspection ensured that this aperture is adequate for photometry, i.e., VDB0-B195D does not show any obvious signal beyond this radius. In addition, this aperture is nearly the same as that adopted by Perina et al. (2009) to determine the cluster's photometry in the $BVRI$ bands, based on the M31 imaging survey of Massey (2006) (see §2.4 below). Therefore, we use an aperture with $r \approx 15''$ for integrated photometry, i.e., $r = 9$ pixels for the 2k×2k thick CCD camera, and $r = 12$ pixels for the 4k×4k thinned CCD camera. VDB0-B195D is projected onto the disk of M31, where the background is bright and fluctuates, potentially as a function of distance from the cluster center. To avoid contamination from background fluctuations, we adopted annuli for background subtraction spanning between 10 and 15 pixels for the 2k×2k thick CCD camera, and from 13 to 20 pixels for the 4×4k thinned CCD camera, both corresponding to $\sim$ 17–26″. While these annuli are spatially as close as possible to the region dominated by cluster light (so that any differences in background flux are minimized), they are wide enough to average out any expected background fluctuations. The calibrated photometry of VDB0-B195D in 15 filters is summarized in column (6) of Table 1, in conjunction with the 1σ magnitude uncertainties, which include uncertainties from the calibration errors of both the M31-1 field standard stars (see for details Fan et al. 2009; Jiang et al. 2003) and 'the secondary standard stars' in common between the M31-1 and M31-7 fields used for calculation of the mean magnitude offsets between the standard and instrumental magnitudes (see for details Fan et al. 2009), as well as those resulting from our DAOPHOT application.

2.4. *Optical broad-band and near-infrared 2MASS photometry of VDB0-B195D*

Four independent sets of photometric data exist for VDB0-B195D. van den Bergh (1969) obtained UBV photometry using observations of the 200-inch Hale telescope, Battistini et al. (1987) performed $UBVR$ photometry based on photographic plates observed with the 152 cm Ritchey-Chrétien $f/8$ telescope of the University of Bologna in Loiano, King & Lupton (1991) obtained UBV photometry for VDB0-B195D using observations with the University of Hawaii's 2.2 m telescope on Mauna Kea using the $f/10$ secondary and coronene-coated 584 × 416 GEC CCD, and Sharov et al. (1995) performed UBV photometry based on photo-electric observations with the 2.6 m Shain telescope of the Crimean Astrophysical Observatory. In addition, in the Revised Bologna Catalogue (RBC) of M31 GCs published by Galleti et al. (2004), the photometric data of VDB0-B195D in optical bands are based on Battistini et al. (1987) and Sharov et al. (1995), and transformed to the reference system of Barmby et al. (2000) by applying offsets derived from objects in common between the relevant catalog and the data set of Barmby et al. (2000). In the RBC, VDB0-B195D was regarded as two objects. We list these photometric data in Table 2 for comparison. Note that, in the latest RBC incarnation (version 3.5, updated on 27 March 2008), VDB0-B195D is included as a single object.

Galleti et al. (2004) also determined 2MASS $JHK_{\rm s}$ photometric magnitudes for VDB0-B195D (transformed to the CIT photometric system; Elias et al. 1982, 1983), which we have included in Table 3. In addition, Perina et al. (2009) realized that VDB0-B195D is a particularly extended object and that it is possible that the photometry of Sharov et al. (1995) (compiled in the RBC) was obtained with apertures that were not large enough to include all of its flux. Therefore, they redetermined its photometric values in the $BVRI$ bands based on the M31 imaging survey of Massey (2006) using an aperture with $r = 14.4''$, which are also listed in Table 3.

From a comparison of the values in Tables 2 and 3, it is clear that the magnitudes of van den Bergh (1969) are brighter, while the results of the three other references are consistent. The magnitudes determined by Perina et al. (2009) are much brighter, however, because of their careful inclusion of all of the cluster's flux. To compare our photometric results with previously published values, we transformed the magnitudes of VDB0-B195D in the BATC intermediate bands to broad-band $UBVRI$-equivalent photometry based on the relation-

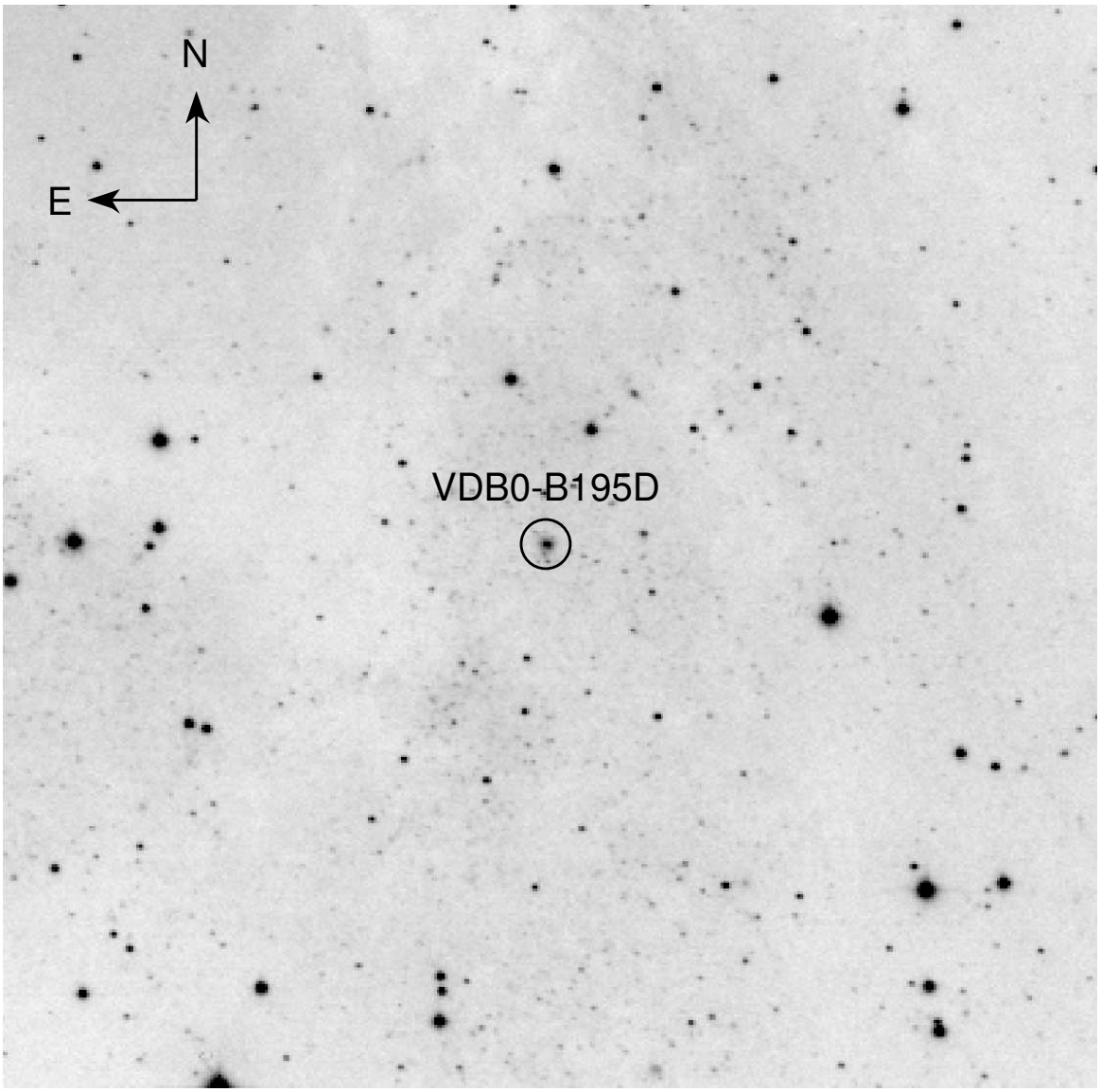

FIG. 1.— Image of VDB0-B195D in the BATC g band, obtained with the NAOC 60/90cm Schmidt telescope. VDB0-B195D is circled using an aperture with a radius of $15''$. The field of view of the image is $11' \times 11'$.

ships obtained by Zhou et al. (2003). These are also listed in Table 3, and the uncertainties include those originating from the transformation based on the relationships of Zhou et al. (2003) and their calibration errors (column 5 of their Table 3). In Fig. 2, we show the result of the comparison. In general, the other photometric data are fainter than ours and those of Perina et al. (2009). Fig. 2 and Table 3 show that our new VRI magnitudes agree with the results of Perina et al. (2009), and that the B magnitude obtained in this paper is 0.32 mag brighter than that of Perina et al. (2009). Considering the photometric errors of both Perina et al. (2009) and our current study, these two B-band photometric results are consistent within 2σ. In addition, we should keep in mind that, although the VRI magnitudes obtained in this paper are consistent with the results of Perina et al. (2009) within 1σ, the disagreement in B magnitudes at this level is understandable. This is caused by the fact that the original photometry in the present paper was obtained in the proprietary BATC filters and transformed to the $UBVRI$ system using transformation equations. Zhou et al. (2003) determined these conversions based on the broad-band $UBVRI$ magnitudes of 48 stars from Landolt (1983, 1992) and Galadí-Enríquez et al. (2000) in the Landolt SA95 field, and their photometric data in the 15 BATC intermediate-band filters. In addition, the central wavelengths and bandwidths of the BATC and $UBVRI$ systems differ. In fact, a similar significant disagreement of B-band photometric data for some M31 GCs was reported by Wang et al. (2010), citing similar arguments.

3. STELLAR POPULATION OF VDB0-B195D

3.1. *Stellar populations and synthetic photometry*

To determine the age and mass of VDB0-B195D, we compared its SED with theoretical stellar population synthesis models. The SED consists of photometric data in the 15 BATC intermediate bands ob-

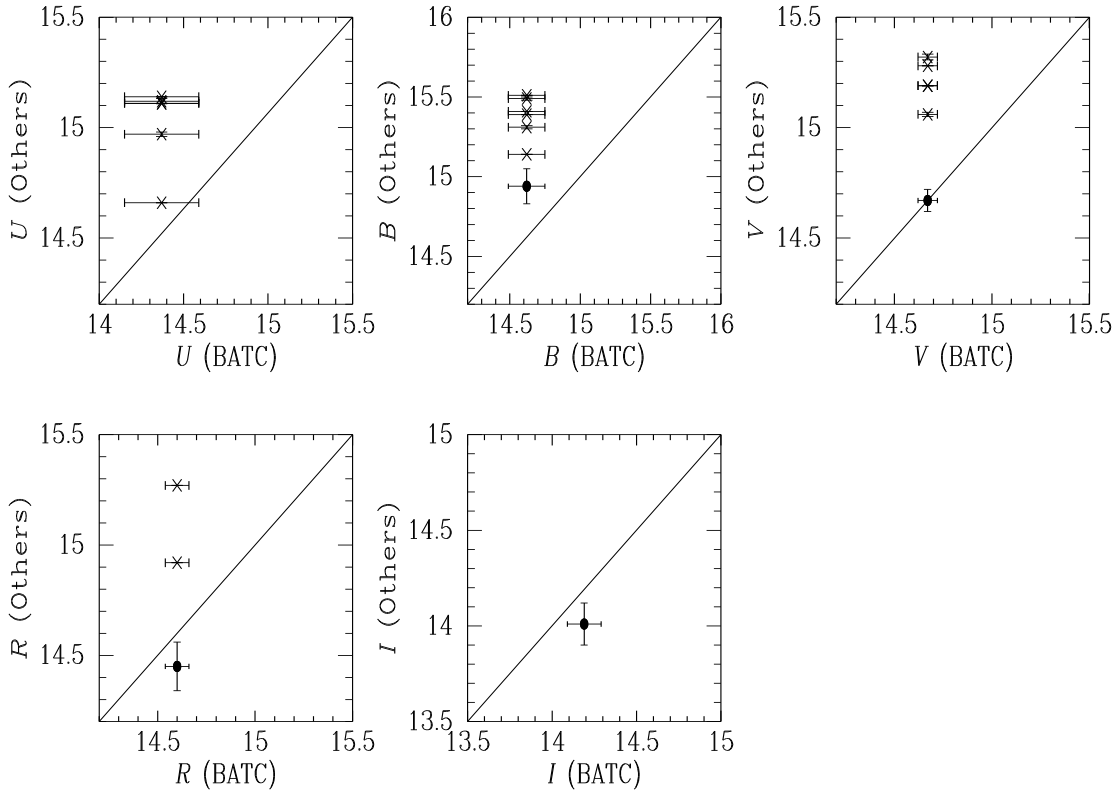

FIG. 2.— Comparison of photometric data from different sources with new determinations in this paper for VDB0-B195D. The data points shown as black dots are from Perina et al. (2009).

tained in this paper and optical broad-band $BVRI$ and 2MASS near-infrared JHK_s data from Perina et al. (2009), listed in Table 3. We used the GALEV SSP models (e.g., Kurth et al. 1999; Schulz et al. 2002; Anders & Fritze-v. Alvensleben 2003) for our comparisons. The GALEV SSPs are based on the Padova stellar isochrones, with the most recent versions using the updated Bertelli et al. (1994) isochrones (which include the thermally pulsing asymptotic giant-branch phase), and a Salpeter (1955) stellar IMF with lower- and upper-mass limits of 0.10 and between 50 and 70 $M_\odot$, respectively, depending on metallicity. The full set of models spans the wavelength range from 91Å to 160 μm. These models cover ages from 4×10^6 to 1.6×10^{10} yr, with an age resolution of 4 Myr for ages up to 2.35 Gyr, and 20 Myr for greater ages. The GALEV SSP models include five initial metallicities, $Z = 0.0004, 0.004, 0.008, 0.02$ (solar metallicity), and 0.05.

Since our observational data consist of integrated luminosities through the set of BATC filters, we convolved the GALEV SSP SEDs with the BATC intermediate-, optical broad-band $BVRI$, and 2MASS filter-response curves to obtain synthetic optical and near-infrared photometry for comparison. The synthetic $i^{\rm th}$ filter magnitude can be computed as

$$m = -2.5 \log \frac{\int_\nu F_\nu \varphi_i(\nu) {\rm d}\nu}{\int_\nu \varphi_i(\nu) {\rm d}\nu} - 48.60, \qquad (1)$$

where F_ν is the theoretical SED and φ_i the response curve of the $i^{\rm th}$ filter of the BATC, $BVRI$, and 2MASS photometric systems. Here, F_ν varies with age and metallicity. Since the observed magnitudes in the $BVRI$ and 2MASS photometric systems are given in the Vega system, we transformed them to the AB system for our fits.

3.2. *Reddening and metallicity of VDB0-B195D*

To obtain the intrinsic SED of VDB0-B195D, its photometry must be dereddened. To date, only Perina et al. (2009) obtained reddening values for VDB0-B195D. They compared the observed CMD with theoretical isochrones and determined $E(B-V) = 0.20 \pm 0.03$ mag. Caldwell et al. (2009) were unable to derive the cluster's reddening value because of the presence of a foreground field star, so they adopted $E(B-V) = 0.28 \pm 0.17$ mag (external rms error), equivalent to the mean reddening of the young clusters in M31. In this paper, we therefore adopt the reddening value from Perina et al. (2009).

In addition, cluster SEDs are affected by age and metallicity effects. Therefore, we can only accurately constrain a cluster's age if the metallicity is known. Perina et al. (2009) found that the CMD of VDB0-B195D, based on their *HST*/WFPC2 observations, is best reproduced by the solar-metallicity models of Girardi et al. (2002). We therefore adopt solar metallicity for VDB0-B195D.

3.3. *The 'lowest-luminosity-limit' test*

The lowest-luminosity limit (LLL; Cerviño & Luridiana 2004) implies that it is meaningless to compare a cluster with population synthesis models to obtain its age and mass if its integrated

luminosity is lower than the luminosity of the most luminous star included in the model for the relevant age. The LLL method states that clusters fainter than this limit cannot be analyzed using standard procedures such as χ^2 minimization of the observed values with respect to the mean SSP models (see also Barker et al. 2008). Below the LLL, cluster ages and masses cannot be obtained self-consistently. To take into account the effects on the integrated luminosities of statistically sampling the stellar IMF (e.g., Cerviño et al. 2000, 2002; Cerviño & Luridiana 2004), we used the theoretical Padova isochrones at http://stev.oapd.inaf.it/cmd (CMD2.2). This interactive Web interface provides isochrones for a number of photometric systems, including optical broad-band, 2MASS, and the BATC data used here. We obtained the solar-metallicity ($Z = 0.019$) isochrones of Marigo et al. (2008), as recommended by CMD2.2, based on the (Salpeter 1955) IMF so as to match the IMF selection for our age and mass determinations of VDB0-B195D in §3.4 (see §3.1 for details).

Figure 3 shows the LLL values as a function of age for the different filters used in this paper. These luminosities are obtained by identifying the most luminous star on each isochrone for the relevant passband. The gray area shows the cluster's absolute luminosity, assuming a distance modulus of $(m-M)_0 = 24.47$ mag (785 kpc) for M31 (McConnachie et al. 2005). The upper luminosity limit has been corrected for extinction, based on a reddening value of $E(B-V) = 0.20$ mag. The interstellar extinction curve, A_λ, is taken from Cardelli et al. (1989), $R_V = A_V/E(B-V) = 3.1$.

We see that VDB0-B195D does not lie below the LLL in any of the passbands used here. This means that, in general, VDB0-B195D can host the most luminous star that would be present theoretically for the given age of the cluster.

3.4. *Fit results*

In the previous section, the LLL test proves that the luminosity of VDB0-195D is higher than the luminosity of its brightest star expected for a given cluster age, i.e., that using SSP models is not completely meaningless. In addition, the bright absolute magnitude of VDB0-195D allows us to consider a possibility that the cluster is massive enough and IMF sampling effects should not strongly impact the fitting results. So we will determine the cluster's age and mass estimates based on direct comparisons with SSP mean values in this section. However, we should keep in mind that this approach is a compromise. In fact, the fitting results (Fig. 4 and Table 5) show probable problem even for relative massive clusters.

We use a χ^2 minimization test to determine which GALEV SSP models are most compatible with the observed SEDs,

$$\chi^2 = \sum_{i=1}^{22} \frac{[m_{\nu_i}^{\rm intr} - m_{\nu_i}^{\rm mod}(t)]^2}{\sigma_i^2}, \qquad (2)$$

where $m_{\nu_i}^{\rm mod}(t)$ is the integrated magnitude in the $i^{\rm th}$ filter of a theoretical SSP at age t (for solar metallicity), $m_{\nu_i}^{\rm intr}$ is the intrinsic, integrated magnitude, and σ_i is the magnitude uncertainty, defined as

$$\sigma_i^2 = \sigma_{{\rm obs},i}^2 + \sigma_{{\rm mod},i}^2 + (R_{\lambda_i} * \sigma_{\rm red})^2 + \sigma_{{\rm md},i}^2. \qquad (3)$$

Here, $\sigma_{{\rm obs},i}$ is the observational uncertainty from column (6) of Table 1 and column (2) of Table 3, $\sigma_{{\rm mod},i}$ is the uncertainty associated with the model itself, $\sigma_{\rm red}$ is the uncertainty in the reddening value, and $R_{\lambda_i} = A_{\lambda_i}/E(B-V)$, where A_{λ_i} is taken from Cardelli et al. (1989), $R_V = A_V/E(B-V) = 3.1$, and $\sigma_{{\rm md},i}$ is the uncertainty in the distance modulus, for the $i^{\rm th}$ filter. Charlot et al. (1996) estimated the uncertainty associated with the term $\sigma_{{\rm mod},i}$ by comparing the colors obtained from different stellar evolutionary tracks and spectral libraries. Following Ma et al. (2007, 2009), we adopt $\sigma_{{\rm mod},i} = 0.05$ mag.

Perina et al. (2009) pointed out that VDB0-B195D is a particularly extended object and that the photometric measurements of van den Bergh (1969), Battistini et al. (1987), King & Lupton (1991), and Sharov et al. (1995) did not include all of its flux. Therefore, we adopt the photometry of Perina et al. (2009) to fit the observed SED with theoretical SSPs for our age determination. The fit yielding the minimum χ^2 value (χ^2(min)) was adopted as the best fit and we adopted the corresponding age value, 60.0 ± 8.0 Myr. In addition, our best-fitting age estimate of 60.0 ± 10.0 Myr results from using the (redder) k–p and $IJHK_{\rm s}$ photometry; using only the blue part of the cluster's SED (B, a–e, where any effects caused by stochasticity may be smaller) yields an age of 72.0 ± 34.0 Myr. The uncertainty was estimated using confidence limits. If $\chi^2/\nu < \chi^2({\rm min})/\nu + 1$, the resulting age is within the 68.3% probability range; here, $\nu = 21$ is the number of free parameters, i.e., the number of observational data points minus the number of parameters used in the theoretical model. Therefore, the accepted age range is derived from those fits that have $\chi^2({\rm min})/\nu < \chi^2/\nu < \chi^2({\rm min})/\nu + 1$. The best reduced-$\chi^2$—defined as $\chi^2_\nu({\rm min}) = \chi^2({\rm min})/\nu$—and age are listed in Table 4. The best fit to the SED of VDB0-B195D is shown in Fig. 4, where we display the intrinsic cluster SED (symbols with error bars), as well as the integrated SED (open circles) and spectrum of the best-fitting model. From Fig. 4, we note that the observational data in the b, d, o, and p BATC filters and in the $K_{\rm s}$ band do not match the best-fitting model very well (the difference is approximately 0.3 mag). Photometric uncertainties in these filters may cause some differences, although this might not be the main reason for the discrepancy. As we know, observational star clusters' SEDs are affected by age, metallicity and reddening. If the reddening value and metallicity adopted in this paper are not problematic, discrepancy between our observations and the best-fitting model may reflect the difficulty in achieving an appropriate (but formal) fit of an SED of a single, real cluster by SSP models. However, as we will see below, the reddening value adopted in this paper may be bigger than the actual reddening of VDB0-B195D. In addition, the differences between the photometric data and the model in Fig. 4 show a somewhat systematic behavior with wavelength: in bluer passbands the cluster seems to be more luminous than predicted by the model, while in redder passbands it is fainter than the corresponding model predictions. A blue excess and red

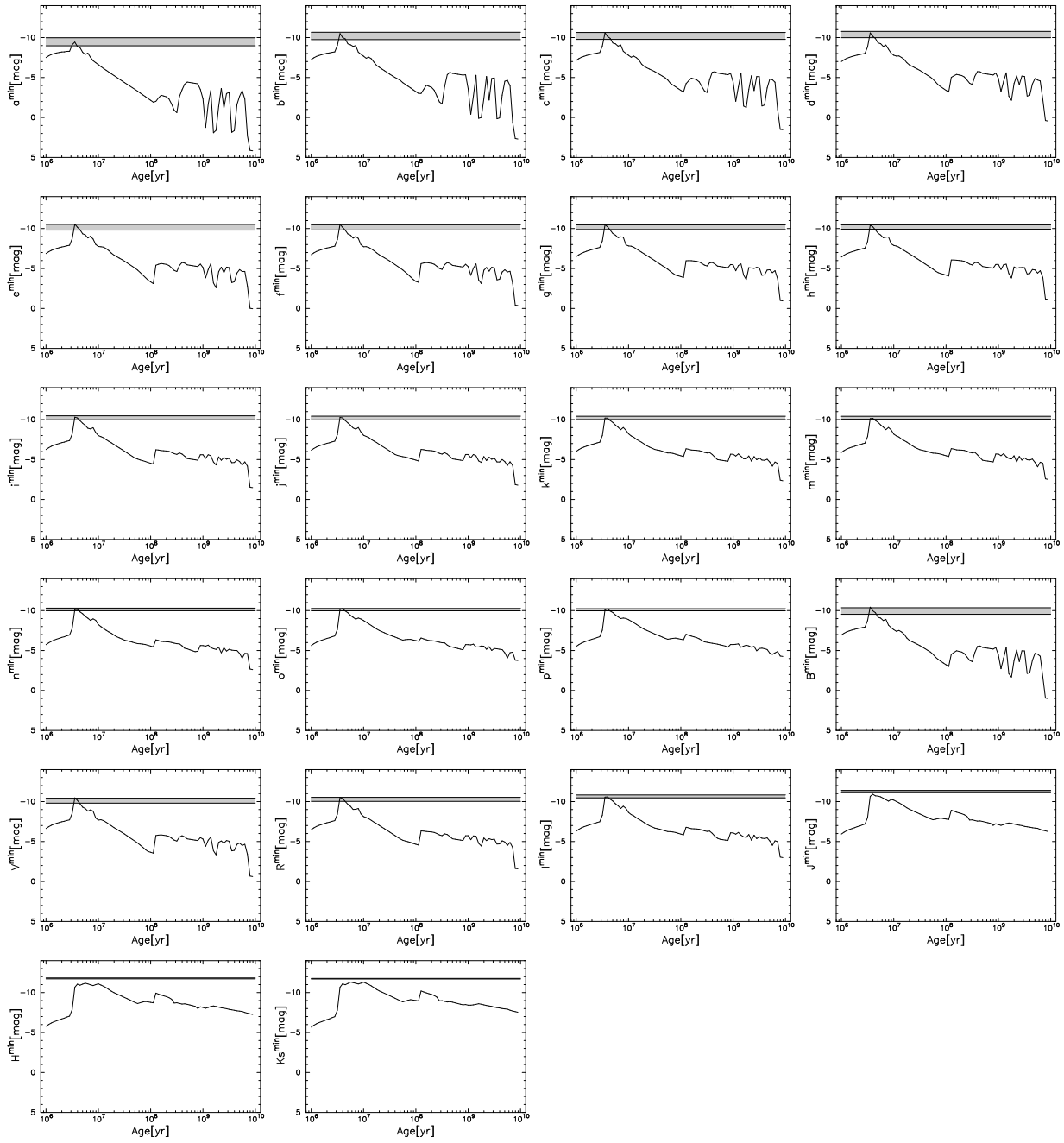

FIG. 3.— Lowest-luminosity limit for the filters used in this paper. The curves indicate the luminosities of the most luminous star on each isochrone for the relevant passband. The light-gray area shows the absolute magnitudes of VDB0-B195D based on a reddening value of $E(B-V) = 0.20$ mag (Perina et al. 2009). We used a distance modulus of $(m-M)_0 = 24.47$ mag (785 kpc) for M31 (McConnachie et al. 2005) to calculate the absolute magnitudes.

deficiency in the observed SED with respect to the model predictions may indicate a shortage of red giants (RGs), which can occur when the cluster is either younger or less massive (or both) than the corresponding best-fitting model suggests. In other words, IMF discreteness may play a role: due to a relatively longer main-sequence (MS) phase and shorter RG phase, a random young cluster is typically bluer than predicted by SSP models. At the same time, we find that the reddening value adopted affects the fitting result greatly. In fact, the best fit to the SED of VDB0-B195D improves a great deal when adopting a smaller reddening value such as $E(B-V)=0.1$: $\chi^2_\nu(\min)=0.73$; the resulting age (64.0 ± 8.0 Myr) is nearly the same as one (60.0 ± 8.0 Myr) obtained with $E(B-V)=0.2$.

We next determined the mass of VDB0-B195D. The GALEV models include absolute magnitudes (in the Vega system) in 77 filters for SSPs of $10^6\ M_\odot$, including 66 filters of the *HST*, Johnson $UBVRI$ (see for details Landolt 1983), Cousins RI (see for details Landolt 1983), and JHK (Bessell & Brett 1988) systems. The difference between the intrinsic absolute magnitudes and those given by the model provides a direct measurement of the cluster mass, in units of $10^6\ M_\odot$. However, we should keep in mind that this is only correct for cluster masses above $10^6\ M_\odot$. We estimated the mass of VDB0-B195D using magnitudes in all of the $BVRI$ and $JHK_{\rm s}$ bands. Therefore, we transformed the 2MASS $JHK_{\rm s}$ magnitudes to the photometric system of Bessell & Brett (1988) using the equations given by Carpenter (2001). The resulting mass determinations for VDB0-B195D are listed in Table 5 with their 1σ uncertainties including contributions from uncertainties in extinction and distance modulus. From Table 5, we see that the mass of VDB0-B195D obtained based on the magnitudes in different filters is very different. (The highest mass obtained, based on the B-band magnitude, is $0.5\times10^5\ M_\odot$ more massive than that obtained using the K_s magnitude.) In addition, the mass estimates differ systematically with filters. Provided that VDB0-B195D is massive enough to be fitted by SSP models, a systematic trend of masses based on different passbands may indicate a problem with reddening value adopted for the cluster. If the actual reddening is smaller than the adopted value, the actual luminosity would be overestimated. This effect is small in redder filters but strong in bluer filters. As discussed in age estimation, a smaller reddening value can improve the fitting result greatly. In fact, a smaller reddening value can reduce the mass discrepancies based on the magnitudes in different filters. When we adopted $E(B-V)=0.1$, the mass of VDB0-B195D obtained based on the magnitudes in different filters is the same within 1σ. We list these estimates in Table 7. From Table 5, we know that the mass of VDB0-B195D obtained in paper is between $(1.1-1.6)\times10^5\ M_\odot$ when the reddening value is adopted to be $(B-V)=0.2$.

4. SUMMARY AND DISCUSSION

VDB0-B195D was previously shown to be a massive cluster based on *HST*/WFPC2 observations. Its color is extremely blue and it is very bright, particularly in blue bands. In addition, VDB0-B195D is an extended object, and most previous photometric measurements did not include its full flux distribution (see Perina et al. 2009, for details).

In this paper, we obtained the cluster's SED in the 15 BATC intermediate-band filters. We subsequently determined its age and mass by comparing our multicolor photometry with theoretical stellar population synthesis models. Our multicolor photometric data consist of 15 intermediate-band filters obtained in this paper, and broad-band $BVRI$ and 2MASS $JHK_{\rm s}$ from Perina et al. (2009), covering a wavelength range from 3000 to 20,000 Å. Our results show that VDB0-B195D is a genuine YMC in M31.

To understand the real nature of the BLCCs, Perina et al. (2009, 2010) performed an *HST* imaging survey of 20 BLCCs in M31's disk. As a test case, Perina et al. (2009) presented details of the data-reduction pipeline that will be applied to all survey data and describe its application to VDB0-B195D. They estimated the object's age, by comparison of the observed CMD with theoretical isochrones from Girardi et al. (2002), at $\simeq25$ Myr. In addition, they constrained realistic upper and lower limits to the cluster's age, independent of the adopted metallicity, within the relatively narrow range from 12 to 63 Myr. Using Maraston's SSP models of solar metallicity (Maraston 1998, 2005), Salpeter (1955) and Kroupa (2001) IMFs, and photometric values in the V and 2MASS J, H, and $K_{\rm s}$ bands, Perina et al. (2009) concluded that the mass of VDB0-B195D is $>2.4\times10^4\ M_\odot$, with their best estimates in the range $\simeq(4-9)\times10^4\ M_\odot$.

Caldwell et al. (2009) presented an updated catalog of 1300 objects in M31, including spectroscopic and imaging surveys, based on images from either the LGGS or the DSS and spectra taken with the Hectospec fiber positioner and spectrograph on the 6.5 m MMT. They derived ages and reddening values for 140 young clusters by comparing their observed spectra with model spectra from the Starburst99 SSP suite (Leitherer et al. 1999). The results show that these clusters are less than 2 Gyr old, while most have ages between 10^8 and 10^9 yr (the age of VDB0-B195D they derive is $\log{\rm age/yr}=7.6$). In addition, Caldwell et al. (2009) also estimated the masses of these young clusters using V-band photometry and model mass-to-light ratios (Leitherer et al. 1999) corresponding to the derived spectroscopic ages. This resulted in masses ranging from 2.5×10^2 to $1.5\times10^5\ M_\odot$. The mass of VDB0-B195D obtained by Caldwell et al. (2009) is $\log M_{\rm cl}/M_\odot=5.1$ (no uncertainty quoted).

We compare the various age and mass estimates of VDB0-B195D in Table 6. Our newly obtained age is older than the estimates of both Perina et al. (2009) and Caldwell et al. (2009), while the mass obtained in this paper is higher than the estimate of Perina et al. (2009) and consistent with the determination of Caldwell et al. (2009). However, our results are in agreement with those of both Perina et al. (2009) and Caldwell et al. (2009) within 3σ. The age and mass obtained in this paper confirms that VDB0-B195D is genuinely a YMC in M31.

As we know, SSP models describe a very special case of a continuous distribution of stellar mass (or light) along isochrones. This is well approximated by clusters with masses larger than $10^6\ M_\odot$. Also, for cluster masses of about $10^5\ M_\odot$, SSP models can probably still be applied since a systematic difference between SSP models and ob-

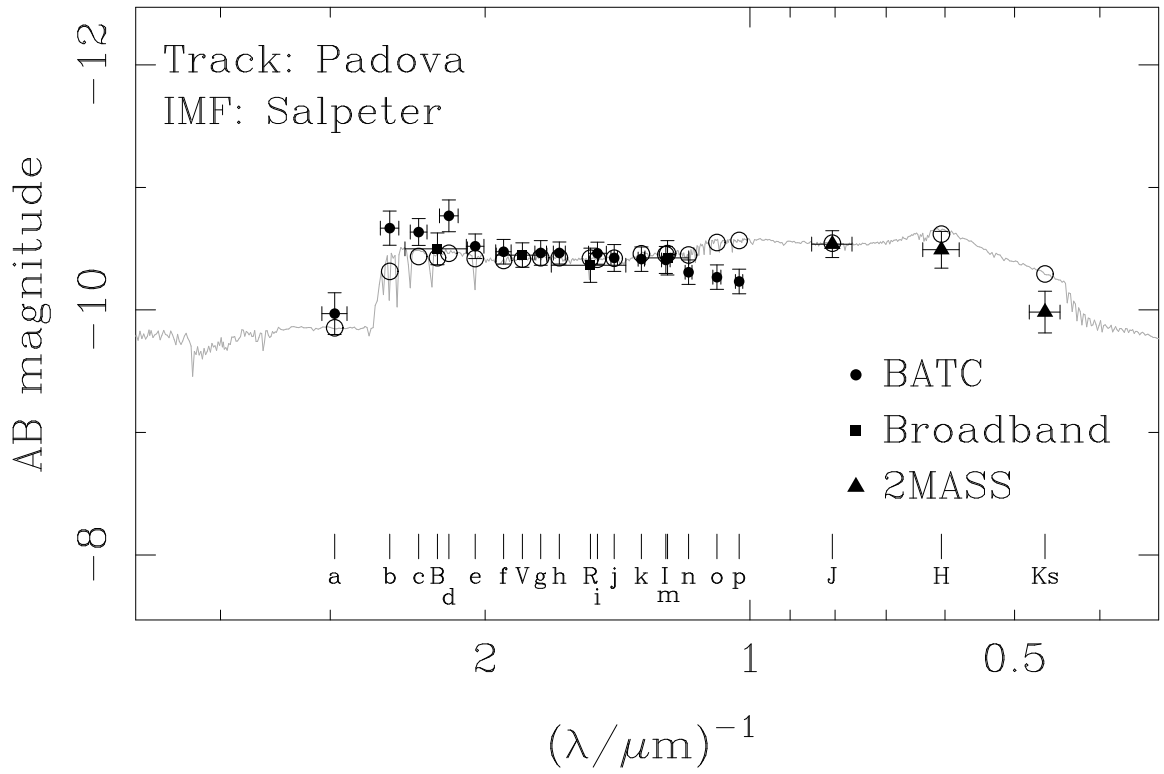

FIG. 4.— Best-fitting, integrated theoretical GALEV SEDs compared to the intrinsic SED of VDB0-B195D. The photometric measurements are shown as symbols with error bars (vertical for uncertainties and horizontal for the approximate wavelength coverage of each filter). Open circles represent the calculated magnitudes of the model SED for each filter. We used a distance modulus of $(m-M)_0 = 24.47$ mag (785 kpc) for M31 (McConnachie et al. 2005) to calculate the absolute magnitudes.

servations should, on average, be smaller than 0.05 mag for clusters older than 10 Myr (see Fig. 3 in Piskunov et al. 2009). However, from the results of this paper, we may conclude that, probably, a formal fitting of SSP models to observed SEDs cannot be used without caution even for relatively massive (or apparently massive) clusters, and it is highly doubtful that this approach can be applied in a routine work providing accurate cluster parameters. The relative accuracy of 10% for age and 20% found for the mass of VDB0-B195D seems to be rather formal and not very confident. In addition, observational star clusters' SEDs are affected by reddening, an effect that is also difficult to separate from the combined effects of age and metallicity (Calzetti 1997; Vazdekis et al. 1997; Origlia et al. 1999). Only the metallicity and reddening are derived accurately (and, ideally, independently), these degeneracies are largely (if not entirely) reduced, and ages can then also be estimated accurately based on a comparison of multicolor photometry spanning a significant wavelength range (de Grijs et al. 2003b; Anders et al. 2004) with theoretical stellar population synthesis models. It is true that the discrepancy between our observations and the best-fitting model is great, and the mass of VDB0-B195D obtained based on the magnitudes in different filters is very different. However, when we adopt a smaller reddening value, the results improve greatly. So, we conclude that the actual reddening value of VDB0-B195D may be smaller than $E(B-V) = 0.2$.

We are indebted to the anonymous referee for very carefully reading our manuscript, and for many thoughtful comments and insightful suggestions that improved this paper significantly. We are grateful to Dr. Richard de Grijs for the help in terms of scientific input and proofreading. This work was supported by the Chinese National Natural Science Foundation (grants 10873016, 10633020, 10603006, and 10803007) and by the National Basic Research Program of China (973 Program), No. 2007CB815403.

REFERENCES

Anders, P., & Fritze-v. Alvensleben, U. 2003, A&A, 401, 1063
Anders, P., Bissantz, N., Fritze-v. Alvensleben, U., & de Grijs, R. 2004, MNRAS, 347, 196
Barker, S., de Grijs, R., & Cerviño, M. 2008, A&A, 484, 711
Barmby, P., Huchra, J., Brodie, J., Forbes, D., Schroder, L., & Grillmair, C. 2000, AJ, 119, 727
Battistini, P., Bònoli, F., Braccesi, A., Fusi Pecci, F., Malagnini, M. L., & Marano, B. 1980, A&AS, 42, 357
Battistini, P., Bònoli F., Braccesi, A., Federici, L., Fusi Pecci, F., Marano, B., & Börngen, F. 1987, A&AS, 67, 447
Battistini, P., Bònoli, F., Casavecchia, M., Ciotti, L., Federici, L., & Fusi Pecci F. 1993, A&A, 272, 77
Beasley, M. A., et al. 2004, AJ, 128, 1623
Bertelli, G., Bressan, A., Chiosi, C., Fagotto, F., & Nasi, E. 1994, A&AS, 106, 275
Bessell, M. S., & Brett, J. M. 1988, PASP, 100, 1134
Bik, A., Lamers, H. J. G. L. M., Bastian, N., Panagia, N., & Romaniello, M. 2003, A&A, 397, 473
Bònoli, F., Delpino, F., Federici, L., & Fusi Pecci, F. 1987, A&A, 185, 25

Brown, T. M., et al. 2004, ApJ, 613, L125
Bruzual, A. G., & Charlot, S. 2003, MNRAS, 344, 1000
Caldwell, N., Harding, P., Morrison, H., Rose, J. A., Schiavon, R., & Kriessler, J. 2009, AJ, 137, 94
Calzetti, D. 1997, AJ, 113, 162
Cao, C., & Wu, H. 2007, AJ, 133, 1710
Cardelli, J. A., Clayton, G. C., & Mathis, J. S. 1989, ApJ, 345, 245
Carpenter, J. M. 2001, AJ, 121, 2851
Cerviño, M., Luridiana, V., & Castander, F. J. 2000, A&A, 360, L5
Cerviño, M., Valls-Gabaud, D., Luridiana, V., & Mas-Hesse, J. M. 2002, A&A, 381, 51
Cerviño, M., & Luridiana, V. 2004, A&A, 413, 145
Charlot, S., Worthey, G., & Bressan, A. 1996, ApJ, 457, 625
Clark, J. S., Negueruela, I., Crowther, P. A., & Goodwin, S. P. 2005, A&A, 434, 949
Crowther, P. A., Hadfield, L. J., Clark, J. S., Negueruela, I., & Vacca, W. D. 2006, MNRAS, 372, 1407
Dubath, P., & Grillmair, C. J. 1997, A&A, 321, 379
de Grijs, R., & Parmentier, G. 2007, ChJAA, 7, 155
de Grijs, R., Bastian, N., & Lamers, H. J. G. L. M. 2003a, MNRAS, 340, 197
de Grijs, R., Fritze-v. Alvensleben, U., Anders, P., Gallagher, J. S., Bastian, N., Taylor, V. A., & Windhorst, R. A. 2003b, MNRAS, 342, 259
de Grijs, R., Anders, P., Lynds, R., Bastian, N., Lamers, H. J. G. L. M., & O'Neill, E. J. Jr. 2003c, MNRAS, 343, 1285
Elias, J. H., Frogel, J. A., Matthews, K., & Neugebauer, G. 1982, AJ, 87, 1029
Elias, J. H., Frogel, J. A., Hyland, A. R., & Jones, T. J. 1983, AJ, 88, 1027
Fan, X., et al. 1996, AJ, 112, 628
Fan, Z., Ma, J., de Grijs, R., Yang Y., & Zhou X. 2006, MNRAS, 371, 1648
Fan, Z., Ma, J., & Zhou X. 2009, RAA, 9, 993
Federici, L., Bonoli, F., Ciotti, L., Fusi Pecci, F., Marano, B., Lipovetsky, V. A., Neizvestny, S. I., & Spassova, N. 1993, A&A, 274, 87
Fusi Pecci, F., Bellazzini, M., Buzzoni, A., De Simone, E., Federici, L., & Galleti, S. 2005, AJ, 130, 554
Galadí-Enríquez, D., Trullols, E., & Jordi, C. 2000, A&AS, 146, 169
Galleti, S., Federici, L., Bellazzini, M., Fusi Pecci, F., & Macrina, S. 2004, A&A, 426, 917
Galleti, S., Bellazzini, M., Federici, L., & Fusi Pecci, F. 2005, A&A, 436, 535
Galleti, S., Federici, L., Bellazzini, M., Buzzoni, A., & Fusi Pecci, F. 2006, A&A, 456, 985
Galleti, S., Bellazzini, M., Federici, L., Buzzoni, A., & Fusi Pecci, F. 2007, A&A, 471, 127
Girardi, L., et al. 2002, A&A, 391, 195
Hiltner, W. A. 1958, ApJ, 128, 9
Hodge, P. W. 1961, ApJ, 133, 413
Hubble, E. P. 1932, ApJ, 76, 44
Huchra, J., Stauffer, J., & van Speybroeck, L. 1982, ApJ, 259, L57
Huchra, J. P., Brodie, J. P., & Kent, S. M. 1991, ApJ, 370, 495
Jablonka, P., Bica, E., Bonatto, C., Bridges, T. J., Langlois, M., & Carter, D. 1998, A&A, 335, 867
Jiang, L., Ma, J., Zhou, X., Chen, J., Wu, H., & Jiang Z. 2003, AJ, 125, 727
Kim, S., et al. 2007, AJ, 134, 706
King, J. R., & Lupton, R. H. 1991, ASP Conf. Ser. 13:, The formation and evolution of star clusters, 13, 575
Kron, G. E., & Mayall, N. U. 1960, AJ, 65, 581
Kroupa, P. 2001, MNRAS, 322, 231 AJ, 65, 581
Kurth, O. M., Fritze-v. Alvensleben, U., & Fricke, K. J. 1999, A&AS, 138, 19
Landolt, A. U. 1983, AJ, 88, 439
Landolt, A. U. 1992, AJ, 104, 340
Larsen, S. S., & Richtler, T. 1999, A&A, 345, 59
Larsen, S. S. 2004, ASP Conf. Ser. 322: The Formation and Evolution of Massive Young Star Clusters, 322, 19
Larsen, S. S., Brodie, J. P., & Hunter, D. A. 2004, AJ, 128, 2295
Lee, M. G., Hwang, H. S., Kim, S. C., Park, H. S., Geisler, D., Sarajedini, A., & Harris, W. E. 2008, ApJ, 674, 886
Leitherer, C., et al. 1999, ApJS, 123, 3
Ma, J., de Grijs, R., Yang, Y., Zhou, X., Chen, J., Jiang, Z., Wu, Z., & Wu, J. 2006, MNRAS, 368, 1443
Ma, J., et al. 2007, ApJ, 659, 359
Ma, J., et al. 2009, AJ, 137, 4884
McConnachie, A. W., Irwin, M. J., Ferguson, A. M. N., Ibata, R. A., Lewis, G. F., & Tanvir, N. 2005, MNRAS, 356, 979
Maraston, C. 1998, MNRAS, 300, 872
Maraston, C. 2005, MNRAS, 362, 799
Marigo, P., Girardi, L., Bressan, A., Groenewegen, M. A. T., Silva,L., & Granato, G. L. 2008, A&A, 482, 883
Massey, P., Olsen, K. A. G., Hodge, P. W., Strong, S, B., Jacoby, G. H., Schlingman, W., & Smith, R. C. 2006, AJ, 131, 2478
Mayall, N. U., & Eggen, O. J. 1953, PASP, 65, 24
Origlia, L., Goldader, J. D., Leitherer, C., Schaerer, D., & Oliva, E. 1999, ApJ, 514, 96
Oke, J. B., & Gunn, J. E. 1983, ApJ, 266, 713
Peacock, M., et al. 2010, MNRAS, 402, 803
Perina, S., et al. 2009, A&A, 494, 933
Perina, S., et al. 2010, A&A, 511, 23
Perrett, K. M., Bridges, T. J., Hanes, D. A., Irwin, M. J., Brodie, J. P., Carter, D., Huchra, J. P., & Watson, F. G. 2002, AJ, 123, 2490
Piskunov, A. E., Kharchenko, N. V., Schilbach, E., Röser, S., Scholz, R. D., & Zinnecker, H. 2009, A&A, 507L, 5
Popescu, B., & Hanson, M. M. 2010, ApJ, 713L, 21
Puzia, T. H., Zepf, S. E., Kissler-Patig, M., Hilker, M., Minniti, D., & Goudfrooij, P. 2002, A&A, 391, 453
Puzia, T. H., Perrett, K. M., & Bridges, T. J. 2005, A&A, 434, 909
Racine, R. 1991, AJ, 101, 865
Rich, R. M., Shara, M. M., & Zurek, D. 2001, AJ, 122, 842
Salpeter, E. E. 1955, ApJ, 121, 161
Schulz, J., Fritze-v. Alvensleben, U., Möller, C. S., & Fricke, K. J. 2002, A&A, 392, 1
Searle, L., Sargent, W. L. W., & Bagnuolo, W. G. 1973, ApJ, 179, 427
Seyfert, C. K., & Nassau, J. J. 1945, ApJ, 102, 377
Sharov, A. S., Lyutyi, V. M., & Esipov, V. F. 1995, SvAL, 21, 240
Stetson, P. B. 1987, PASP, 99, 191
Tinsley, B. M. 1968, ApJ, 151, 547
Tinsley, B. M. 1972, ApJ, 178, 319
Vazdekis, A., Peletier, R. F., Beckman, J. E., & Casuso, E. 1997, ApJS, 111, 203
van den Bergh, S. 1969, ApJS, 19, 45
Vetešnik, M. 1962, Bull. Astron. Inst. Czech., 13, 182
Wang, S., Fan, Z., Ma, J., de Grijs, R., & Zhou, X. 2010, AJ, 139, 1438
Williams, B. F., & Hodge, P. W. 2001a, ApJ, 548, 190
Williams, B. F., & Hodge, P. W. 2001b, ApJ, 559, 851
Yan, H. J., et al. 2000, PASP, 112, 691
Zheng, Z. Y., et al. 1999, AJ, 117, 2757
Zhou, X., et al. 2003, A&A, 379, 361

TABLE 1
BATC photometry of the M31 YMC VDB0-B195D.

Filter	Central wavelength (Å)	Bandwidth (Å)	Number of images	Exposure time (hours)	Magnitude
a	3360	222	6	2.0	15.51 ± 0.14
b	3890	187	6	2.0	14.73 ± 0.11
c	4210	185	3	0.8	14.70 ± 0.07
d	4550	222	3	1.0	14.49 ± 0.10
e	4920	225	3	1.0	14.67 ± 0.05
f	5270	211	3	1.0	14.65 ± 0.05
g	5795	176	3	1.0	14.59 ± 0.04
h	6075	190	3	1.0	14.56 ± 0.02
i	6660	312	3	1.0	14.50 ± 0.02
j	7050	121	5	1.7	14.51 ± 0.06
k	7490	125	3	1.0	14.47 ± 0.05
m	8020	179	3	1.0	14.43 ± 0.07
n	8480	152	6	2.0	14.49 ± 0.05
o	9190	194	6	2.0	14.49 ± 0.05
p	9745	188	6	2.0	14.50 ± 0.05

TABLE 2
Comparison of broad-band photometry of VDB0-B195D.

Filter	Mag[a]	Mag[b]	Mag[c]	Mag[d]	Mag[e]	Mag[f]
U	14.66	15.11	15.12 ± 0.012	14.97 ± 0.01	15.110	15.140
B	15.14	15.39	15.49 ± 0.010	15.31 ± 0.01	15.410	15.510
V	14.94	15.19	15.32 ± 0.013	15.06 ± 0.01	15.190	15.280
R		15.27			14.920	

[a]van den Bergh (1969); [b]Battistini et al. (1987); [c]King & Lupton (1991), uncertainties are the median uncertainties in the mean for all sample cluster measurements; [d]Sharov et al. (1995); [e]Photometry from Galleti et al. (2004), based on Battistini et al. (1987); [f]Photometry from Galleti et al. (2004), based on Sharov et al. (1995).

TABLE 3
Recently determined photometry for VDB0-B195D.

Filter	Mag[a]	Mag[b]	Mag[c]
U			14.37 ± 0.22
B	14.94 ± 0.09		14.62 ± 0.13
V	14.67 ± 0.05		14.67 ± 0.05
R	14.45 ± 0.11		14.60 ± 0.06
I	14.01 ± 0.11		14.19 ± 0.10
J	13.26 ± 0.07	13.78 ± 0.03	
H	12.76 ± 0.12	13.15 ± 0.04	
K_s	12.77 ± 0.15	12.96 ± 0.03	

[a]Perina et al. (2009); [b]Galleti et al. (2004); [c]This paper.

TABLE 4
Age estimate of VDB0-B195D based on the the galev models.

Age (Myr)	log (Age) [yr]	χ^2_ν(min) (per degree of freedom)
60.0 ± 8.0	7.78 ± 0.05	2.2

TABLE 5
Mass estimates (and uncertainties) of VDB0-B195D based on the galev models.

B	V	R	I	J	H	K_s
Mass (10^5 $M_\odot$)						
1.6 ± 0.18	1.6 ± 0.13	1.4 ± 0.17	1.4 ± 0.16	1.4 ± 0.13	1.3 ± 0.16	1.1 ± 0.17

TABLE 6
Comparison of age and mass estimates of VDB0-B195D.

Age[1] (Myr)	Age[2] (Myr)	log (Age)[3] [yr]	log (Age)[2] [yr]	Mass[1] (10^4 $M_\odot$)	Mass[2] (10^5 $M_\odot$)	log (Mass)[3] [$M_\odot$]	log (Mass)[2] [$M_\odot$]
25	60.0 ± 8.0	7.6	7.78 ± 0.05	$4 - 9$	$1.1 - 1.6$	5.1	$5.0 - 5.2$

[1]Perina et al. (2009); [2]This paper; [3]Caldwell et al. (2009).

TABLE 7
Mass estimates (and uncertainties) of VDB0-B195D based on the galev models with $E(B-V) = 0.1$.

B	V	R	I	J	H	K_s
Mass (10^5 $M_\odot$)						
1.1 ± 0.12	1.2 ± 0.10	1.1 ± 0.14	1.2 ± 0.14	1.3 ± 0.12	1.2 ± 0.16	1.1 ± 0.17